Desalination and Water Treatment
www.deswater.com
doi: 10.1080/19443994.2015.1020511

57 (2016) 8204–8216
April

Taylor & Francis
Taylor & Francis Group

Applications of innovative configurations of double absorption heat transformers in water purification technology

Mehrdad Khamooshi[a,*], Kiyan Parham[a], Iman Roozbeh[b], Hamed Ensafisoroor[c]

[a]*Department of Mechanical Engineering, Eastern Mediterranean University, G. Magosa, Mersin 10, North-Cyprus, Turkey, Tel. +98 915 305 0362; Fax: +90 392 3653715; email: mehrdadkhamooshi@yahoo.com (M. Khamooshi), Tel. +90 533 876 1435; email: kiyan.parham@emu.edu.tr (K. Parham)*
[b]*Department of Industrial Engineering, Eastern Mediterranean University, G. Magosa, Mersin 10, North-Cyprus, Turkey, Tel. +90 392 630 2821; Fax: +90 392 3653715; email: iman.roozbeh@cc.emu.edu.tr*
[c]*School of Mechanical Science and Engineering, Huazhong University of Science and Technology, Hongshan District, Wuhan, Hubei 430074, P.R. China, email: hamedensafi1@yahoo.com*

Received 15 July 2014; Accepted 7 February 2015

ABSTRACT

In this study, first law of thermodynamics has been employed to analyze the performances of two different configurations of double absorption heat transformers (DAHTs) in water purification system. The upgraded heat in the absorber of the absorption heat transformers provides the heat for desalination process. The first investigated configuration is the most efficient DAHT according to the literature, and the second one is a novel configuration proposed by the authors. The aim of this research was to investigate the effects of different parameters on the studied configurations of DAHTs and the desalination system and to compare their performances in detail. Additionally by considering the quantity of the produced water, both the configurations were optimized. The results revealed that the proposed configuration is capable of producing freshwater for 806 residual units.

Keywords: Absorption heat transformer; Double; LiBr + H_2O; Desalination; Crystallization risk; COP

1. Introduction

The global demand for high quality drinking water has become a major challenge during last decades. The main reasons are environmental concerns in terms of air pollution, global warming, emission of greenhouse gasses, and reduction of annual rainfalls which is Earth's main freshwater source. Additionally, for the reason of increasing the world's population and rapid economic development, the necessity for potable water has grown significantly [1].

Desalination processes used in water purification industry have become more popular, due to their capability of providing freshwater from extensively available salty water in the oceans. The distillation setup can separate water form dissolved substances by evaporating and then condensing it once more [2]. Detecting and providing thermal energy sources for desalination systems have become an imperative subject for researchers throughout decades. This thermal energy source can be provided by solar energy, or other additional heat sources [3]. On the other hand, huge amounts of low- or mid-level waste heat are

*Corresponding author.

released daily from industrial processes to the atmosphere [4]. Some industrial cycles have demonstrated the capability of utilizing these waste heats in more useful applications.

Organic Rankine cycle (ORC) and CO_2 transcritical power cycle are good samples of them which can efficiently convert low-temperature waste heat into electricity [5,6]. But in desalination systems, the temperature of the mid-level waste heat should be increased. Absorption heat transformers (AHTs), which are talented in upgrading the energy efficiency of industrial applications, appear to be an outstanding choice for utilizing these waste heats. They are systems with opposite operation processes of absorption heat pumps (AHPs).

Considering the fact that fundamentals of the AHTs are similar to those of AHPs, they have the same advantages including, quite operation, low maintenance requirement, low mechanical work input, and simple design [4,7–9].

The schematic diagram of a single-stage absorption heat transformer (SAHT) is shown in Fig. 1. It consisted of a generator, a condenser, an evaporator, an absorber, a heat exchanger, and an expansion valve. The operating system of the single absorption heat transformer is explained as follows:

Heat is transferred to solution of $LiBr/H_2O$ in the generator and to the refrigerant in the evaporator from the waste heat of an industrial unit. Superheated water vapor comes out from the generator and then enters to the condenser wherein it is condensed as saturated liquid. The pressure of the water is then raised to that of evaporator through pump. In the evaporator, water is heated and vaporized. This vapor is then absorbed in the absorber by strong solution of $LiBr/H_2O$ coming back from generator (state 10).

The weak $LiBr/H_2O$ solution (with lower concentration of LiBr) from the absorber goes to the generator by means of solution heat exchanger economizer (ECO) and the expansion valve, respectively. The released heat from the absorber is at a temperature range of 100–140˚C. This upgraded energy can now be used in the water purification system.

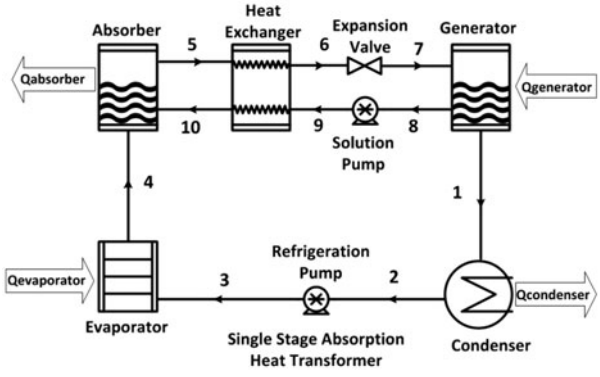

Fig. 1. Schematic view of single absorption heat transformer [10].

The difference between the upgraded temperature in the absorber and the input heat in the evaporator is called gross temperature lift ($GTL = T_{abs} - T_{eva}$). The amount of GTL basically depends on the additional stages added to the SAHTs. The GTL of 50˚C and coefficient of performance (COP) nearby 0.5 are accessible by applying a single absorption heat transformer [11]. A double absorption heat transformer (DAHT) can increase the GTL to 80˚C, but the COP decreases to 0.36 [12]. Triple absorption heat transformers (TAHT) are capable of enhancing the temperature even to 140˚C higher than the source temperature [13].

Different configurations of the single absorption heat transformer with LiBr/H2O were investigated by Horuz and Kurt [4]. It was concluded that modified configurations could increase the COP by 14.1% in comparison with those of basic absorption heat transformers. Parham et al. [14] simulated and optimized the same configurations used in [4] while they were integrated to a water desalination process. It was revealed that the best setup is capable of producing enough water for 2,100 residential units. Zare et al. [15] utilized the waste heat from a gas turbine-modular helium reactor to produce power through two ORCs and an AHT for producing pure water by means of distillation processes. They demonstrated that the COP and the water production rate had direct relations with the heat source temperature of the AHT. Yari et al. [16] proposed and analyzed a combined cogeneration cycle in which the waste heat from an ejector-expansion trans-critical CO_2 refrigeration cycle was utilized for power production and water purification, simultaneously. The waste heat utilization was performed by means of a CO_2 supercritical power cycle and a desalination system for pure water production. It was found that, under the optimized conditions, the energy efficiency ratio of the combined cogeneration cycle was about 13–45% higher than the COP of the ejector-expansion trans-critical CO_2 cycle without AHT and desalination system. Huicochea et al. [17] investigated the integration of a SAHT into a water purification system. A fraction of the obtained heat from an auxiliary condenser was recycled into the heat source temperature. They showed that, once the concentration of the solution in the absorber increased, COP_{AHT}, COP_{WP}, and the quantity of distilled water enhanced. A comparative study for the performance prediction of a SAHT coupled into water desalination system was made by Hernandez

et al. [18]. They utilized neural network model (NnM) and thermodynamic model in their simulations and concluded that the NnM model executed better. Gomri analyzed and evaluated the performances of the single- and double-effect absorption heat transformer systems in seawater desalination [19]. The results revealed higher amounts of COP and exergetic coefficient of performance (ECOP) for the double-effect absorption heat transformer than that of SAHT. On the contrary, the pure water production rate for single-effect configuration was higher than that of double effect. Energy and exergy analysis of a DAHT operating with LiBr/H_2O was studied by Martinez and Rivera [12]. They developed a mathematical model for estimating the COP, ECOP, and exergy destruction in all components of the system. Horuz and Kurt [20] compared the performances of single, series, and parallel DAHTs when used for sea water desalination and reported that the latter system is preferred from the view point of water production. Donnellan et al. [13] introduced six different configurations of TAHTs applying H_2O/LiBr as the working pair. They analyzed and optimized the number and places of internal heat exchanger units within the system using heat exchangers network modeling. Khamooshi et al. [21] applied the latter-mentioned setups in desalination system and indicated that the optimized amount of distilled water produced by the best configuration could supply potable water for 1,131 residential units. Later, they applied first law of thermodynamics to analyze and optimize the performance of a TAHT operating with LiBr/H_2O as the working pair, in more detail [22]. Parham et al. [23] performed a comprehensive review on different absorption heat transformer technologies and systems. The performance of the absorption cycles depends not only on their configurations, but also on thermodynamic properties of working pairs which are regularly composed of refrigerants and absorbents [24–26]. Sun et al. [27] conducted a review study about different types of working pairs in absorption cycles. Furthermore, Khamooshi et al. [10] did a similar work for the employed ionic liquids as the working fluids in absorption cycles.

Rivera et al. [28] studied the performance of a single-stage heat transformer operating with the water/lithium bromide and the water/CarrolTM mixtures theoretically and experimentally. It was observed that almost the same tendencies and values of the COP and flow ratio are obtained in general for both mixtures. However, because of the higher solubility of the water/Carrol mixture, the SAHT operated over a larger range of generator and evaporator temperatures and with higher gross temperature lifts.

Zhao et al. [29] introduced a new type of DAHT in which the temperature of the absorbing evaporator was not an independent variable and system's degrees of freedom was less than that of the DAHT with other solution cycles by one. The results showed that in comparison with the other types of DAHTs, the new type of DAHT had higher COP especially when absorber's temperature gets higher. However, their study did not investigate the effects of most of the major parameters on the performance of the system and they simply introduced the setup. In this paper, a novel DAHT cycle coupled to a water desalination system has been proposed, analyzed, and compared with the latter-mentioned DAHT which stands as the most optimized configuration. The proposed cycle is in essence a simplified version of the previously designed TAHT by Donnellan et al. [13].

A thorough analysis of the first law of thermodynamics will be performed for both of the configurations. A parametric study is carried out and validated by other studies available from literature in order to identify the effects of some parameters such as the temperatures of the condenser, evaporator, absorber, generator, and absorber/evaporator (AB/EV) on the COP, utilized heat for desalination, and quantity of distilled water.

2. System description

Fig. 2 shows a DAHT integrated to a water desalination system, introduced by Zhao et al. [29] which will be denoted as configuration 1 within this paper. It is obvious that a DAHT consists of a SAHT with an additional stage containing AB/EV.

The operation sequences of the mentioned DAHT are as follows:

The industrial waste heat is supplied to separate the refrigerant (H_2O) from the solution (H_2O + LiBr) in the generator in an intermediate temperature of T_{GE}. The refrigerant leaves the generator to the condenser where it is condensed to its saturated level. Then, the condensed working fluid is split into two streams. One portion is pumped to the evaporator where it is vaporized at an intermediate temperature of T_{EV} and pressure of P_{EV}. The second half of the stream is pumped at a higher pressure (P_{AB}) and vaporized in the AB/EV. The vaporized working fluid is absorbed in the absorber at a higher temperature (T_{AB}) by the strong solution X_{GE} coming from the generator. The weak solution coming back from the absorber is fed to AB/EV to absorb the vaporized working fluid coming from the evaporator and to deliver an amount of $Q_{AB/EV}$. The water purification system receives its required thermal energy from the absorber of the AHT system.

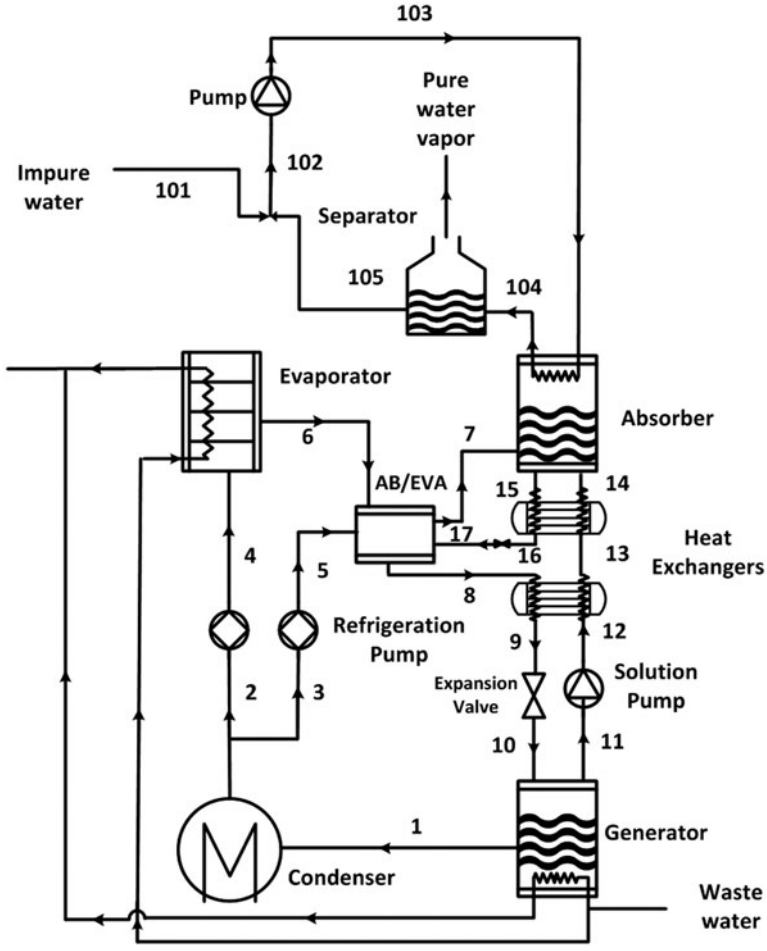

Fig. 2. Schematic view of the first configuration DAHT integrated to water desalination (configuration 1).

The impure water is heated in the absorber where it is partially evaporated. The two phase flow enters the separator vessel where it is separated into liquid and vapor. The liquid water mixes with the entering impure water before returning to the suction pump.

Fig. 3 shows the proposed DAHT integrated to a water desalination system (configuration 2). The difference between configurations 1 and 2 arises in the distribution of solution out coming from the generator.

As demonstrated in Fig. 3, in the second configuration, the absorber has two separated lines of strong solutions flowing out from the generator for absorbing the refrigerant, but in first setup, the weak solution of the absorber becomes the strong solution for absorbing the refrigerant in AB/EV.

3. Thermodynamic analysis

This section describes the thermodynamics model used for the simulation of the studied DAHTs. Each component of the considered systems has been treated as a control volume, and the principles of mass and energy conservation are applied to it. Engineering equation solver (EES) is used for solving the equations [30].

3.1. Assumptions

The simulation was performed according to the following assumptions:

(1) Changes in kinetic and potential energies are negligible [13,14,31].
(2) The pressure losses due to the frictional effects in the connecting pipes of the AHT are ignored [12–14,31].
(3) The system is in thermodynamic equilibrium, and all the processes are assumed to be steady flow processes [12,14].
(4) Some proper values of effectiveness are considered for the heat exchangers [12–14,31].

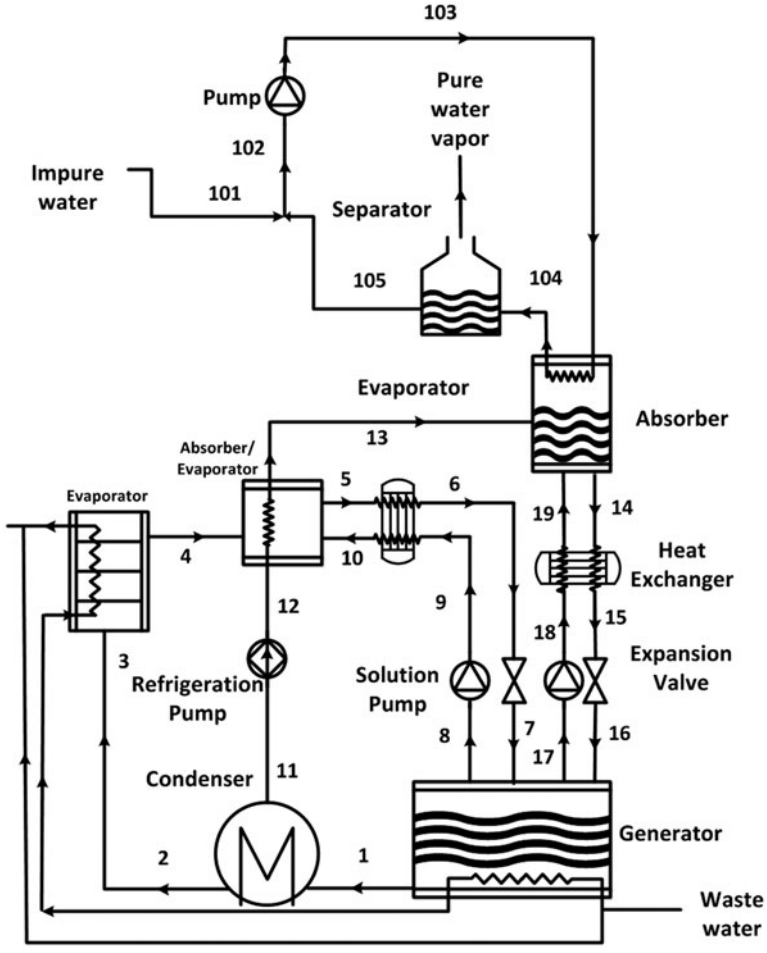

Fig. 3. Schematic view of the proposed DAHT integrated to water desalination (configuration 2).

(5) The solution at the generator and the absorber outletsand the refrigerant at the condenser and the evaporator outlets are all at saturated states [12–14,31].
(6) Heat losses from components are very small relative to heat fluxes and are thus not included in the model [12–14,31].
(7) The evaporator and the generator of the AHT operate at the same temperature [12,14].
(8) The refrigerant vapor is assumed to evaporate and condense completely in the absorber-evaporators, the evaporator, and the condenser [12–14,31].
(9) The heat source for the AHT system is the hot water generated by a cogeneration system in a textile company. The industrial system has four different units, each of them producing 15 ton/h water at 90 ± 2°C [4,14].
(10) The mechanical energy consumed by pumps is neglected [14].
(11) The freshwater is salt free [14].
(12) Absorber heat is transferred to impure water as latent and sensible heat [14,15].

3.2. Performance evaluation

Table 1 summarizes the basic assumptions and input parameters used in the simulation.

The COP is a measure of a cycle's ability to transfer heat at various temperature levels [39]:

$$\mathrm{COP} = \frac{\dot{Q}_{\mathrm{abs}}}{\dot{Q}_{\mathrm{gen}} + \dot{Q}_{\mathrm{eva}}} \tag{1}$$

where $\dot{Q}_{\mathrm{abs}}$, $\dot{Q}_{\mathrm{gen}}$, and $\dot{Q}_{\mathrm{eva}}$ correspond, respectively, to the heat capacities and inputs in absorber, generator, and evaporator (Table 2).

Another important parameter which is absolutely imperative for designing and optimizing absorption

Table 1
The input data of simulation

Parameters	Value
T_{con} (℃)	20–35[a]
T_{abs} (℃)	140–165[b]
T_{eva} (℃)	75–90[c]
$T_{eva} = T_{gen}$ (℃)	[d]
$T_{AB/EV1}$ (℃)	110–130[e]
$T_{heat\ source}$ (℃)	90 ± 2℃[f]
m-dot heat source (ton/h)	60[f]
ε_{ECO} (%)	80[g]

Where the values are obtained from literature as follows:
[a][32–34].
[b][12,29,35].
[c][12,29,35].
[d][14,19,36,37].
[e][12,29,35].
[f][4,14].
[g][14,19,38].

cycles is flow ratio. It is defined as the ratio of the total mass flow rate of weak solution entering the generator to the mass flow rate of refrigerant vapor leaving the generator [13]:

$$f = \frac{\text{mass flow of salt solution entering the generator}}{\text{mass flow of vapor leaving the generator}} \tag{2}$$

The amount of the utilized heat for desalination $Q_{utilized}$ is also a critical parameter [14]:

$$\dot{Q}_{Utilized} = \dot{m}_{104}(h_{104} - h_{103}) \tag{3}$$

3.3. Model validation

As mentioned earlier, basically a conventional DAHT is founded on a SAHT with additional stages. So, herein, initially the available data in the literature for SAHTs have been used for verifying the present model. The obtained results from our simulation have been compared with the results of Rivera et al. [34]. It was assumed that the heat and pressure losses in the pipes are negligible, the expansion valve is isenthalpic, and the effectiveness of the ECO is 70%.

Fig. 4 shows the comparison between the COP obtained from the present work with the one reported by Rivera et al. [34]. It illustrates the fact that our results are in high coherence with experimental data and our simulations are validated.

Table 2
Heat capacities of the main components for different configurations

Heat capacities	Evaporator	Generator	Condenser	Absorber	AB/EV$_1$
Cases 1	$\dot{Q}_{eva} = \dot{m}_{18}(h_{18} - h_{19}) = \dot{m}_6(h_6 - h_4)$	$\dot{Q}_{gen} = \dot{m}_1 h_1 + \dot{m}_{11} h_{11} - \dot{m}_{10} h_{10}$	$\dot{Q}_{con} = \dot{m}_1 h_1 - \dot{m}_2 h_2 - \dot{m}_3 h_3$	$\dot{Q}_{abs} = \dot{m}_7 h_7 + \dot{m}_{14} h_{14} - \dot{m}_{15} h_{15}$	$\dot{Q}_{AB/EV} = \dot{m}_5(h_7 - h_5) = \dot{m}_6 h_6 + \dot{m}_{17} h_{17} - \dot{m}_8 h_8$
Case 2	$\dot{Q}_{eva} = \dot{m}_{20}(h_{20} - h_{21}) = \dot{m}_4(h_4 - h_3)$	$\dot{Q}_{gen} = \dot{m}_1 h_1 + \dot{m}_8 h_8 + \dot{m}_{17} h_{17} - \dot{m}_7 h_7 - \dot{m}_{16} h_{16}$	$\dot{Q}_{con} = \dot{m}_1 h_1 - \dot{m}_2 h_2 - \dot{m}_{11} h_{11}$	$\dot{Q}_{abs} = \dot{m}_{13} h_{13} + \dot{m}_{19} h_{19} - \dot{m}_{13} h_{13}$	$\dot{Q}_{AB/EV} = \dot{m}_{12}(h_{13} - h_{12}) = \dot{m}_4 h_4 + \dot{m}_{10} h_{10} - \dot{m}_5 h_5$

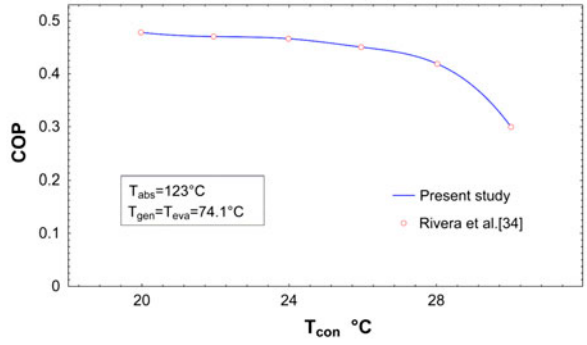

Fig. 4. Validation of SAHT configuration with experimental data.

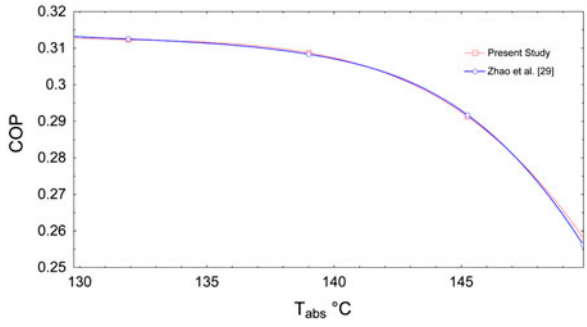

Fig. 5. The effect of T_{abs} on COP for configuration 1 in comparison with that of reported in [29].

As the second validation case, a basic DAHT is validated with the results stated by Zhao et al. [29].

The assumptions are as follows:

(1) $T_{eva} = T_{gen} = 70$ ℃.
(2) $T_{con} = 35$ ℃.
(3) $T_{AB/EV} = 110$ ℃.

The modified configuration will be validated by comparing the result of this work with the Zhao et al's. study.

Fig. 5 shows the effect of absorber temperature on the COP of the same system. The consistency and similarity between the obtained result of the current work and the results from the Zhao's study [29] once again show the validation of the system.

4. Results and discussion

The main parameters of the two studied setups of DAHTs such as energy transfer rate, concentration, COP, distilled water, and the utilized heat at the same input conditions are summarized and compared in Table 3.

The effects of T_{abs} on the COP, distilled water, and utilized heat in desalination for the both configurations are presented in Figs. 6 and 7. It is evident that the performance of the second configuration is more sensible to absorber's temperature in comparison with the first one. The highest quantity of COP, distilled water, and utilized heat for configuration 2 occur within the midrange of the absorber's temperature. The same trend is observed for the COP of the configuration 1, but the quantity of freshwater and utilized heat decreases by increasing the absorber's temperature. This is in agreement with those of reported in [12,29]. Figs. 6 and 7 emphasize the fact that the behavior of the utilized heat is the same as the trend of distilled water. Once more, first configuration performs better and has higher amount of utilized heat compared to the second configuration.

Table 3
The comparison of input and calculated properties of the two studied configurations of DAHTs

	Unit	Configuration 1	Configuration 2
Absorber temperature (T_{abs})	℃	165	165
Condenser temperature (T_{con})	℃	30	30
Absorber/Evaporator temperature ($T_{AB/EV}$)	℃	130	130
Generator temperature (T_{gen})	℃	80	80
Evaporator temperature (T_{eva})	℃	80	80
COP	–	0.3071	0.2927
$\dot{Q}_{Utilized}$	kW	219.5	197
Weak solution concentration (X_w)	–	0.4943	0.4943
Strong solution concentration (X_s)	–	0.6294	0.6294
Distilled water	kg/s	0.08583	0.07663

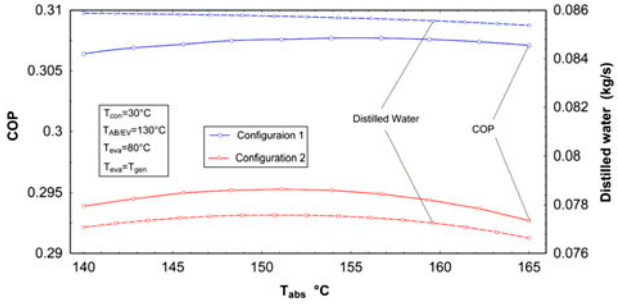

Fig. 6. Effect of T_{abs} on COP and distilled water for two different configurations.

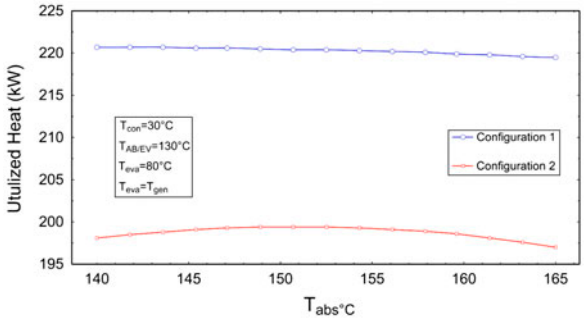

Fig. 7. Effect of T_{abs} on utilized heat of two different configurations.

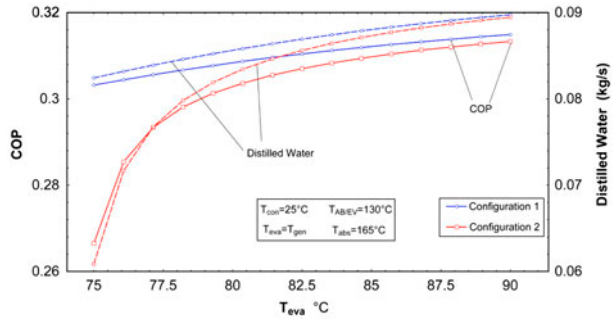

Fig. 8. Effect of T_{eva} on the COP and distilled water for two different configurations.

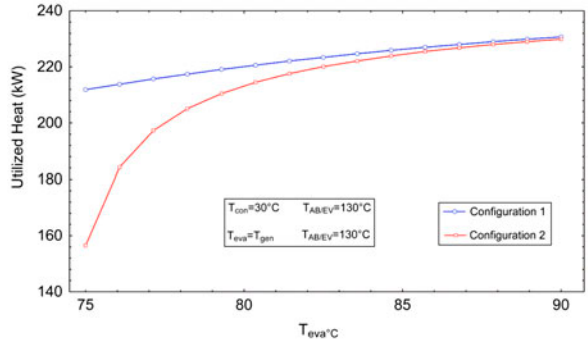

Fig. 9. Effect of T_{eva} on the utilized heat of two different configurations.

The influence of evaporator's temperature on the COP, distilled water, and utilized heat is shown in Figs. 8 and 9. It is clear that as the evaporator temperature increases, the COP and quantity of freshwater also increase. This is due to the fact that increasing evaporator temperature (and pressure) leads to a lower weak solution concentration and flow ratio (f). The lower flow ratio results in a higher absorption heat capacity and as a result higher COP [12,14,20]. At lower evaporator temperatures, the performance of the second configuration is slightly poor and increasing T_{eva} improves both the COP and produced distilled water. While evaporator's temperature rises from 75 to 90°C, the amount of utilized heat for configuration 2 increases from 156 to 230 kW, which reveals 47% increment growth. However, this progress percentage for the first configuration is totally minor compared to that of the second setup.

The effect of condenser's temperature on the COP of the systems is presented in Fig. 10.

As shown, by increasing condenser's temperature, COPs for the both setups are decreasing.

Once more, configuration 1 performs better. The COP of the second configuration decreases considerably at higher condenser temperatures. The reason is the fact that by increasing condenser's temperature, the minimum system pressure increases and the concentration of the strong solution would decrease. This leads to a growth in flow ratio and thus lowers absorber heat capacity. These consequences are approved earlier in references [12,20].

In Fig. 11, COPs of the two configurations are depicted vs. variation of absorber/evaporator temperature. In configuration 1, COP decreases by increasing the temperature of $T_{AB/EV}$, because of the latter-mentioned reason which states that increasing the temperature of the absorber/evaporator decreases the heat capacity of the absorber. Since the structure of the two configurations is different in the absorber/evaporator component, their behavior is totally different as displayed in Fig. 11. The optimum temperature of absorber/evaporator in the second configuration is the same as that of conventional TAHT which is around midpoint temperature between the highest and lowest possible setting [31].

The concentration of the working pair including LiBr and H_2O in AHT systems is mainly classified in

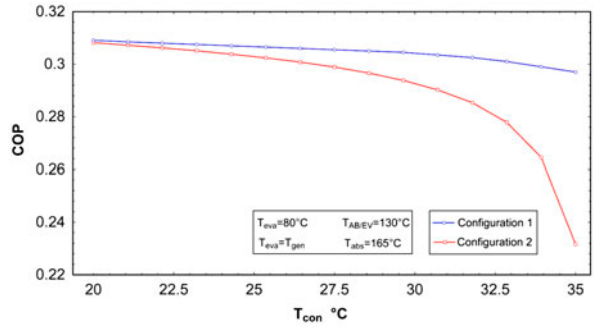

Fig. 10. Effect of T_{con} on the COP of two different configurations.

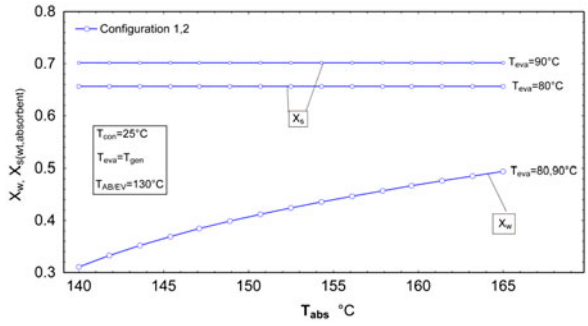

Fig. 12. Effects of absorber temperatures on X_s and X_w for different configurations at two different evaporation temperatures.

two categories: strong solution (X_s, from the generator to the absorber) and weak solution (X_w, from the absorber to the generator). In Fig. 12, both the X_s and X_w are plotted against the absorber temperature. It is apparent that while generating, condensing, and absorbing/evaporating temperatures are kept constant, X_s does not vary with $T_{abs,}$ but X_w increases. For higher evaporator or generator temperatures, the strong solution is higher. Flow ratio is directly dependent on X_s which can cause a LiBr crystallization problem [4,14,15]. Thus, it can be concluded that higher evaporator and generator temperatures enhance the risk of crystallization in the DAHTs.

The concentration difference ($\Delta X = X_s - X_w$) exhibits a parabolic decrease with increasing absorber temperature as shown in Fig. 13. As reported in the literature [15,40], once T_{gen}, T_{eva}, $T_{AB/EV}$, and T_{con} are not varying, the ΔX and T_{abs} changes as a function of flow ratio (f), which can be controlled simply. Higher f also results in higher $T_{abs,}$ mechanical power losses, and also higher possibility of crystallization within working fluid. It is evident that lower evaporator temperature leads to lower ΔX which is absolutely a satisfactory outcome according to Fig. 13. This is in agreement with the results of Horuz [4] which indicated that an AHT operates better at higher T_{eva}.

As mentioned earlier, performances of absorption cycles depend on several parameters. Utilization of ECO's seems to be totally essential for improving the performances of DAHTs and more water production while employed in desalination.

The performance indicator of an ECO is its effectiveness which is defined for any ECO. As Fig. 14 demonstrates, both the COP and distilled water are dependent on the economizer's effectiveness. In the second configuration, as ECO's effectiveness increases from 0.1 to 0.8, an increment percentage of about 57% is witnessed. On the other hand, this growth rate for the first configuration is around 12%.

Each configuration has two internal heat exchangers. Identifying the importance of the heat exchangers on the performance of the cycle is of great significance. Using the EES, the effectiveness of each heat exchanger is kept as low as possible ($\varepsilon_{ECO} = 0.1$), while the other parameters have their usual values. Table 4 shows the effect of each heat exchanger on the performance of the systems. Obviously, the first heat exchanger in configuration 2 has the highest impact on the performance of the system compared to other heat exchangers.

Input variables: T_{con} = 30˚C, $T_{gen} = T_{eva}$, T_{eva} = 80˚C, $T_{AB/EV}$ = 130˚C, T_{abs} = 165˚C.

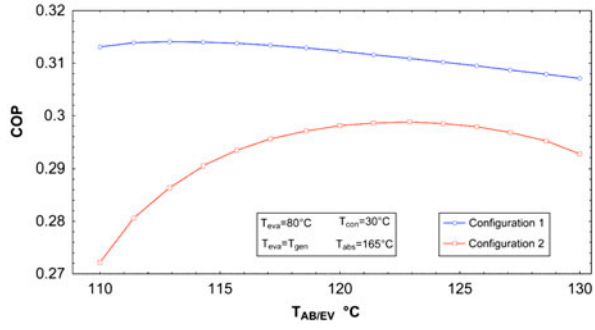

Fig. 11. Effect of $T_{AB/EV}$ on the COP of two different configurations.

5. Optimization

Parametric analyses show that the quantity of the freshwater mainly depends on the temperatures of the generator, evaporator, AB/EV, and absorber. Therefore, the optimum quantity of freshwater output of the system can be expressed as a function of five design parameters as shown in the following equation:

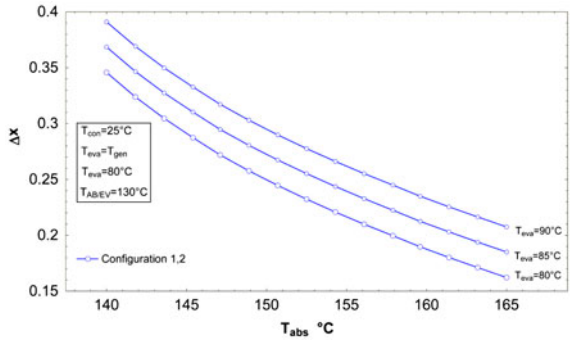

Fig. 13. Effects of absorber temperature on ΔX for different configurations at three different evaporation temperatures.

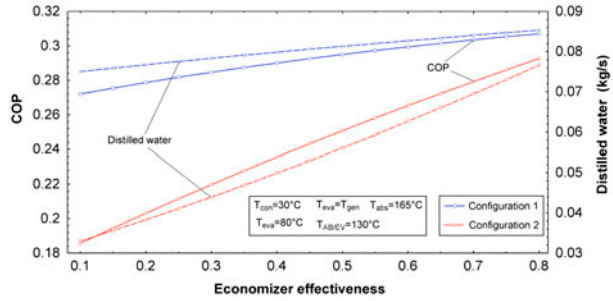

Fig. 14. Effects of ECO effectiveness on COP and distilled water for the both configurations.

Table 4
The comparison of the effects of each heat exchanger on the performance of the systems

	HEX1	HEX2	COP	Distilled water (kg/s)
Configuration 1	0.8	0.8	0.3071	0.08538
	0.1	0.8	0.2944	0.07758
	0.8	0.1	0.2956	0.08470
Configuration 2	0.8	0.8	0.2927	0.07633
	0.1	0.8	0.2168	0.40440
	0.8	0.1	0.2523	0.06250

Table 5
Optimization results for configuration 1

T_{eva} (℃)	T_{con} (℃)	$T_{AB/EV}$ (℃)	T_{gen} (℃)	T_{abs} (℃)	X_s	X_w	COP	Q_u(kW)	Distilled water (kg/s)
80	24.83	120	80	160.6	0.6574	0.5265	0.3152	231.8	0.09019
82	24.99	120	82	160.3	0.6657	0.5252	0.3167	234	0.09103
84	25.05	120	84	160.4	0.6745	0.5259	0.3179	235.9	0.09178
86	25.03	120	86	160.2	0.6837	0.5245	0.3189	237.2	0.09230
88	25.15	120	88	160.5	0.6922	0.5259	0.3198	238.6	0.09281
90	25.15	120	90	160.3	0.7013	0.5250	0.3204	239.3	0.09308

Table 6
Optimization results for configuration 2

T_{eva} (℃)	T_{con} (℃)	$T_{AB/EV}$ (℃)	T_{gen} (℃)	T_{abs} (℃)	X_s	X_w	COP	Q_u (kW)	Distilled water (kg/s)
80	25	120	80	149.9	0.6565	0.5489	0.3103	224.6	0.08739
82	25	120	82	150.6	0.6657	0.5384	0.3125	227.7	0.08859
84	25	120	84	151	0.6747	0.5276	0.3139	229.7	0.08937
86	25	120	86	151.6	0.6839	0.5166	0.3150	231.3	0.09000
88	25	120	88	152.3	0.6929	0.5053	0.3160	232.6	0.09051
90	25	120	90	152.5	0.7018	0.4935	0.3168	233.7	0.09090

$$\text{Maximize } \dot{m}_{\text{distilledwater}}(T_{\text{gen}}, T_{\text{eva}}, T_{\text{con}}, T_{\text{AB/EV1}}, T_{\text{AB/EV2}}, T_{\text{abs}})$$

Subject to:

$$25 \leq T_{\text{con}} \leq 35^{\circ}\text{C}, \quad 80 \leq T_{\text{eva}} \leq 90^{\circ}\text{C},$$
$$80 \leq T_{\text{gen}} \leq 90^{\circ}\text{C}, \quad 120 \leq T_{\text{AB1/EV1}} \leq 140^{\circ}\text{C},$$
$$140 \leq T_{\text{abs}} \leq 165^{\circ}\text{C}$$

The performance of the whole cycle is optimized by applying direct search method (DSM), assuming the distilled water as the objective function. DSM is a well-known iterative optimization technique which does not using any approximation of gradients. The history of the DSM arises from the 1960s, and since then, it became very popular in optimization procedures. It was applied for solving economic and engineering problems [41]. DSM is popular as an unconstrained optimization technique that does not explicitly use derivatives [42].

In this study, optimization was performed by assuming six different constant evaporator temperatures. The objective of the optimization was finding the maximum freshwater production rate for each configuration. Additionally, the temperatures of the main components were set as constraints as discussed earlier.

5.1. Optimization results

By raising evaporator's temperature ($T_{\text{eva}} = T_{\text{gen}}$), the COP and freshwater production rate increase for both the configurations which is completely in agreement with Figs. 9 and 10. Comparing the studied configurations, the first one shows better performance and has higher freshwater output. The maximum amount of obtained COP and quantity of distilled water from configuration 1 are 0.3204 and 0.09308, respectively. All the optimization results are in coherence with the results presented in the earlier figures. As Tables 5 and 6 indicate, the condensation temperature should be kept as low as possible which is in agreement with the earlier discussions of Fig. 11. By increasing T_{eva}, a growth in COP and freshwater production rate is witnessed.

Jradi et al. [43] demonstrated that each typical residential requires 10 L of freshwater per day. Therefore, assuming that configuration 1 operates nonstop, it will be able to produce enough water for 806 residential units.

6. Conclusion

A thermodynamic analysis of two different configurations of DAHTs integrated into a water desalination system was studied. The aim of the research was to analyze and compare the performance of a novel configuration of DAHT with the most efficient one available in the literature. Additionally, an optimization was made in the EES by considering the quantity of the distilled water as the objective function. It was discovered that the first configuration shows better performance due to the variation of the main parameters such as temperature of the main components and ECO effectiveness compared to the conventional model. The proposed model should perform under the optimized range of temperature to achieve suitable performance. Also, based on results of the analysis and optimization, the following main conclusions are drawn:

(1) The performance of the proposed setup is more sensible to absorber's temperature in comparison with the first one.
(2) By increasing condenser's temperature, COPs for the both setups are decreasing.
(3) Absorber/evaporator temperature for the first configuration should be around the lowest possible setting and as for the second system, it should be close to the midpoint of the highest and lowest possible setting.
(4) First heat exchanger in configuration 2 has the highest impact on the performance of the system compared to other heat exchangers.
(5) The proposed configuration is capable of producing freshwater for 806 residual units.

References

[1] S. Sekar, R. Saravanan, Experimental studies on absorption heat transformer coupled distillation system, Desalination 274 (2011) 292–301.
[2] H.Ş. Aybar, F. Egelioğlu, U. Atikol, An experimental study on an inclined solar water distillation system, Desalination 180 (2005) 285–289.
[3] H. Ensafisoroor, M. Khamooshi, F. Egelioglu, K. Parham, An experimental comparative study on different configurations of basin solar still, Desalin. Water Treat. (2014) 1–16.
[4] I. Horuz, B. Kurt, Absorption heat transformers and an industrial application, Renew. Energ. 35 (2010) 2175–2181.
[5] C. Guo, X. Du, L. Yang, Y. Yang, Performance analysis of organic Rankine cycle based on location of heat transfer pinch point in evaporator, Appl. Therm. Eng. 62 (2014) 176–186.
[6] M. Li, J. Wang, S. Li, X. Wang, W. He, Y. Dai, Thermo-economic analysis and comparison of a CO_2 transcritical power cycle and an organic Rankine cycle, Geothermics 50 (2014) 101–111.
[7] I. Horuz, A comparison between ammonia-water and water-lithium bromide solutions in vapor absorption refrigeration systems, Int. Commun. Heat Mass Transfer 25 (1998) 711–721.

[8] S. Smolen, M. Budnik-Rodz, Low rate energy use for heating and in industrial energy supply systems—Some technical and economical aspects, Energy 31 (2006) 2252–2267.
[9] A. Sözen, H.S. Yücesu, Performance improvement of absorption heat transformer, Renew. Energ. 32 (2007) 267–284.
[10] M. Khamooshi, K. Parham, U. Atikol, Overview of ionic liquids used as working fluids in absorption cycles, Adv. Mech. Eng. 5 (2013).
[11] W. Rivera, R. Best, J. Hernández, C.L. Heard, F.A. Holland, Thermodynamic study of advanced absorption heat transformers—I. Single and two stage configurations with heat exchangers, Heat Recovery Syst. CHP 14 (1994) 173–183.
[12] H. Martínez, W. Rivera, Energy and exergy analysis of a double absorption heat transformer operating with water/lithium bromide, Int. J. Energ. Res. 33 (2009) 662–674.
[13] P. Donnellan, E. Byrne, K. Cronin, Internal energy and exergy recovery in high temperature application absorption heat transformers, Appl. Therm. Eng. 56 (2013) 1–10.
[14] K. Parham, M. Yari, U. Atikol, Alternative absorption heat transformer configurations integrated with water desalination system, Desalination 328 (2013) 74–82.
[15] V. Zare, M. Yari, S.M.S. Mahmoudi, Proposal and analysis of a new combined cogeneration system based on the GT-MHR cycle, Desalination 286 (2012) 417–428.
[16] M. Yari, V. Zare, S.M.S. Mahmoudi, Parametric study and optimization of an ejector-expansion TRCC cycle integrated with a water purification system, Proc. Inst. Mech. Eng., Part A: J. Power Energ. 227 (2013) 383–398.
[17] A. Huicochea, J. Siqueiros, R.J. Romero, Portable water purification system integrated to a heat transformer, Desalination 165 (2004) 385–391.
[18] J.A. Hernández, R.J. Romero, D. Juárez, R.F. Escobar, J. Siqueiros, A neural network approach and thermodynamic model of waste energy recovery in a heat transformer in a water purification process, Desalination 243 (2009) 273–285.
[19] R. Gomri, Thermal seawater desalination: Possibilities of using single effect and double effect absorption heat transformer systems, Desalination 253 (2010) 112–118.
[20] I. Horuz, B. Kurt, Single stage and double absorption heat transformers in an industrial application, Int. J. Energ. Res. 33 (2009) 787–798.
[21] M. Khamooshi, K. Parham, F. Egelioglu, M. Yari, H. Salati, Simulation and optimization of novel configurations of triple absorption heat transformers integrated to a water desalination system, Desalination 348 (2014) 39–48.
[22] M. Khamooshi, K. Parham, M. Yari, F. Egelioglu, H. Salati, S. Babadi, Thermodynamic analysis and optimization of a high temperature triple absorption heat transformer, Sci. World J. 2014 (2014) 10.
[23] K. Parham, M. Khamooshi, D.B.K. Tematio, M. Yari, U. Atikol, Absorption heat transformers—Comprehensive review, Renew. Sustain. Energ. Rev. 34 (2014) 430–452.
[24] K. Parham, U. Atikol, M. Yari, O.P. Agboola, Evaluation and optimization of single stage absorption chiller using ($LiCl + H_2O$) as the working pair, Adv. Mech. Eng. 5 (2013).
[25] W. Chen, S. Liang, Y. Guo, D. Tang, Thermodynamic analysis of an absorption system using [bmim] Zn_2Cl_5/NH_3 as the working pair, Energy Convers. Manage. 85 (2014) 13–19.
[26] D.S. Ayou, M.R. Currás, D. Salavera, J. García, J.C. Bruno, A. Coronas, Performance analysis of absorption heat transformer cycles using ionic liquids based on imidazolium cation as absorbents with 2,2,2-trifluoroethanol as refrigerant, Energ. Convers. Manage. 84 (2014) 512–523.
[27] J. Sun, L. Fu, S. Zhang, A review of working fluids of absorption cycles, Renew. Sustain. Energ. Rev. 16 (2012) 1899–1906.
[28] W. Rivera, R.J. Romero, M.J. Cardoso, J. Aguillón, R. Best, Theoretical and experimental comparison of the performance of a single-stage heat transformer operating with water/lithium bromide and water/Carrol™, Int. J. Energ. Res. 26 (2002) 747–762.
[29] Z. Zhao, Y. Ma, J. Chen, Thermodynamic performance of a new type of double absorption heat transformer, Appl. Therm. Eng. 23 (2003) 2407–2414.
[30] S.A. Klein, F. Alvarado, Engineering Equation Solver, version 9.237, F-Chart Software, (2012, Middleton).
[31] P. Donnellan, E. Byrne, J. Oliveira, K. Cronin, First and second law multidimensional analysis of a triple absorption heat transformer (TAHT), Appl. Energy 113 (2014) 141–151.
[32] R. Best, W. Rivera, Thermodynamic design-data for absorption heat transformers 6. Operating on water carrol, Heat Recovery Syst. CHP 14 (1994) 427–436.
[33] M.A.R. Eisa, R. Best, F.A. Holland, Thermodynamic design data for absorption heat transformers—Part II. Operating on water-calcium chloride, J. Heat Recovery Syst. 6 (1986) 443–450.
[34] W. Rivera, J. Cerezo, R. Rivero, J. Cervantes, R. Best, Single stage and double absorption heat transformers used to recover energy in a distillation column of butane and pentane, Int. J. Energ. Res. 27 (2003) 1279–1292.
[35] Z. Zhao, X. Zhang, X. Ma, Thermodynamic performance of a double-effect absorption heat-transformer using TFE/E181 as the working fluid, Appl. Energ. 82 (2005) 107–116.
[36] R.J. Romero, J. Siqueiros, A. Huicochea, Increase of COP for heat transformer in water purification systems. Part II—Without increasing heat source temperature, Appl. Therm. Eng. 27 (2007) 1054–1061.
[37] J. Siqueiros, R.J. Romero, Increase of COP for heat transformer in water purification systems. Part I—Increasing heat source temperature, Appl. Therm. Eng. 27 (2007) 1043–1053.
[38] R. Gomri, Energy and exergy analyses of seawater desalination system integrated in a solar heat transformer, Desalination 249 (2009) 188–196.
[39] W. Rivera, M.J. Cardoso, R.J. Romero, Single-stage and advanced absorption heat transformers operating with lithium bromide mixtures used to increase solar pond's temperature, Sol. Energ. Mater. Sol. Cells 70 (2001) 321–333.
[40] L. Garousi Farshi, S.M. Seyed Mahmoudi, M.A. Rosen, Analysis of crystallization risk in double effect absorption refrigeration systems, Appl. Therm. Eng. 31 (2011) 1712–1717.

[41] D. Zhang, G.H. Lin, Bilevel direct search method for leader-follower problems and application in health insurance, Comput. Oper. Res. 41 (2014) 359–373.
[42] T.G. Kolda, R.M. Lewis, V. Torczon, Optimization by direct search: New perspectives on some classical and modern methods, SIAM Rev. 45 (2003) 385–482.
[43] M. Jradi, N. Ghaddar, K. Ghali, Experimental and theoretical study of an integrated thermoelectric-photovoltaic system for air dehumidification and fresh water production, Int. J. Energ. Res. 36 (2012) 963–974.